JAAS

ROYAL SOCIETY OF CHEMISTRY

PAPER

View Article Online
View Journal

Cite this: DOI: 10.1039/d5ja00507h

High-precision measurement of Sn isotopic compositions in cassiterite and igneous rock reference materials by double-spike technique using MC-ICP-MS/MS

Da-Peng Zhu, * Edith Kubik, Hans Keppler and Audrey Bouvier

Tin (Sn) isotopic analysis offers profound insights into geochemical and cosmochemical processes, as well as into metallurgical history or archeometry. Yet the accurate determination of Sn isotopic composition is hindered by Sn volatilization, the resistance of cassiterite to dissolution, and purification-induced fractionation. We present a protocol to obtain high-precision Sn isotopic ratios using a ^{117}Sn–^{122}Sn double spike technique and a Thermo Fisher Scientific Neoma multi-collector inductively coupled plasma-mass spectrometer equipped with a collision/reaction cell and pre-cell mass filter (MC-ICP-MS/MS). Tin was purified from sample matrices with a specific ion exchange resin, while minimizing evaporation steps and mitigating isotope loss. Evaporation–re-dissolution tests show that pure Sn solution suffers substantial losses at elevated temperatures, whereas mineral and rock sample matrices stabilize Sn with near-quantitative recoveries up to 120 °C. Concentration mismatch tests reveal a positive linear relationship between sample-to-standard concentration ratios and $\delta^{122/118}Sn_{3161a}$, with $\delta^{122/118}Sn_{3161a}$ offsets limited to less than 0.02‰ when the ratios were in the 0.90–1.10 range. Long-term reproducibility for $\delta^{122/118}Sn_{3161a}$, yielded 0.017‰ (2SD, n = 71 over 10 months), while in-house Sn standards gave 0.029‰ (2SD, n = 22). The Sn isotope compositions of geological reference materials (BCR-2, BHVO-2, AGV-2, GSP-2, W-2, and JA-2) obtained with this protocol show high reproducibility and agree well with reports in other studies. Furthermore, we applied an NaOH fusion-based dissolution method for the acid-resistant mineral cassiterite (SnO_2), which enables efficient and complete digestion of this phase. The Sn isotope composition of cassiterite dissolved using NaOH is consistent with that of samples dissolved using the traditional KCN-based digestion. Our results demonstrate that the double-spike protocol provides accurate, reproducible Sn stable isotope measurements and establishes a robust framework for future applications in geochemistry, cosmochemistry, and archaeometry.

Received 18th December 2025
Accepted 30th March 2026

DOI: 10.1039/d5ja00507h

rsc.li/jaas

1 Introduction

Tin (Sn) is characterized by its low melting point (231.9 °C), high electrical conductivity, corrosion resistance, and anti-friction properties, which make it a key material for plating, soldering, inclusion in the composition of alloys, and electronic applications. The lithophile, moderately siderophile, chalcophile, and moderately incompatible geochemical behavior of Sn makes it a versatile tracer widely applied in both geochemistry and cosmochemistry.[1–4] Tin has ten naturally stable isotopes providing the most extensive mass range from ^{112}Sn to ^{124}Sn, including seven isotopes with natural abundances between ~5% and ~32%. Mass-dependent and mass-independent variations of stable isotopes are responsible for the observed Sn isotopic variations during geological and cosmochemical processes.[3–10] Mass-dependent fractionation can arise during Earth's differentiation, magma differentiation, and fluid exsolution from melts, as well as in archaeometric contexts, operating under either equilibrium conditions or kinetic regimes (*e.g.*, evaporation and condensation).[3,11–14] Differences in stellar nucleosynthetic production and photochemical reactions in the solar nebula that may induce nuclear field shifts or nuclear spin effects[15,16] can generate mass-independent variations and offer valuable insights into the isotopic behavior of Sn.[7,9,17,18] Owing to its strong affinity for both silicate and sulfide phases, Sn isotopes are sensitive tracers of redox-controlled metal partitioning among melt, fluid, and mineral phases, providing constraints on oxidation states and fluid evolution in granite-related systems.[19–21] Furthermore, the moderate volatility and combined siderophile–chalcophile character of Sn make its isotopic system a valuable tool for investigating metal segregation and volatile loss during planetary accretion and differentiation.[3,6,7,14,22]

Universität Bayreuth, Bayerisches Geoinstitut, 95440 Bayreuth, Germany. E-mail: Dapeng.Zhu@uni-bayreuth.de

Since Sn has a high ionization potential (7.3 eV)[23] and volatility, the advancement of multi-collector inductively coupled plasma-mass spectrometry (MC-ICP-MS) technology enables greater precision in Sn isotopic measurements (0.01–0.04‰ per amu) as compared to thermal ionization mass spectrometry (TIMS) (0.12–0.17‰ per amu).[23–35] The double spike technique is a well-established method for correcting isotope fractionation during sample preparation, chromatographic purification, and mass spectrometry. By adding a mixture of two isotopically enriched spikes to the sample prior to chemical treatment, the method enables simultaneous quantification of natural isotopic variations and correction of mass-dependent fractionation introduced throughout analytical procedures. This approach has been successfully applied to high-precision isotope analyses of metals such as Fe,[36] Ni,[37] Zn,[38] and Ge,[39] and is increasingly used for Sn isotopes.[29–35] Over the past ten years, more than 20 studies on Sn isotope analytical methods have been reported, employing different instrument types and purification procedures, and using or not using a double spike technique to correct for isotope mass fractionation during sample processing and analysis.[23,29–35,40–42]

Cassiterite, the principal Sn-bearing mineral in tin ore deposits, provides critical insights into ore-forming mechanisms during magmatic–hydrothermal processes, as indicated by its complex zoning patterns and intergrowth textures.[43–49] The Sn isotope compositions of cassiterite vary both among different deposits and within a single crystal, with differences of up to 0.5‰ per amu (ref. 22, 30 and 50–52) and 0.08‰ per amu (ref. 46, 53 and 54), respectively. Although several mechanisms have been proposed to explain the observed Sn isotope compositions in cassiterite, mainly equilibrium fractionation related to temperature and redox conditions, and kinetic fractionation during rapid crystal growth or fluid evolution, significant debate persists regarding their relative contribution and the specific conditions under which each process dominates. The determination of accurate and precise Sn isotopic ratios in cassiterite and rock samples is a prerequisite for advancing our understanding of Sn mineralization.[39,41,43–48] Cassiterite poses significant analytical challenges because of its resistance to acid digestion. Various techniques have been employed to digest cassiterite, including conventional wet chemistry methods using acid and base digestion. Other techniques have been employed to achieve its dissolution, including graphite crucibles,[55] CO, Na_2CO_3/CO, Cu/CO, CuO/CO,[42] and HI.[23] These methods often fail to fully dissolve cassiterite, reflecting the exceptional chemical resilience of SnO_2. Cassiterite is usually digested in a graphite crucible with KCN at temperatures above 800 °C, a method designed to minimize Sn loss and, consequently, stable isotope fractionation associated with volatilization (SnO or SnH_4) observed when using other techniques.[23,56,57] However, this method is problematic due to the extreme toxicity of KCN. She *et al.* 2023 (ref. 46) proposed using HCl in microwave digestion vessels or conventional Parr bombs for cassiterite digestion. They reported that isotopic fractionation can be avoided only when yields exceed at least 60%. However, the procedure is time-consuming, requiring up to 20 days at 200 °C to reach approximately 80% dissolution. These limitations highlight the need for safer, faster, and more effective dissolution protocols for cassiterite.

The Thermo Fisher Scientific Neoma MC-ICP-MS/MS, equipped with a novel pre-cell double Wien filter that uses combined magnetic and electrostatic fields to guide ion beams, has emerged as a promising platform for high-precision Sn isotopic analysis. A previous study has reported Sn isotope analyses using a Neoma MC-ICP-MS under dry plasma conditions, using the ^{117}Sn–^{122}Sn double spike technique and a Cetac Aridus III desolvation system, without employing the MS/MS functionality.[34] Growing interest in Sn isotopes – stimulated by the substantial fractionations revealed in recent pioneering studies[5,10,11,51] – underscores the need for continued technical work aimed at ensuring data quality and refining procedures for sample preparation and measurement. This requirement is particularly relevant for Sn, a challenging element for which a range of analytical protocols and reference materials have been employed across laboratories.

In this study, we established a high-precision and accurate Sn isotope protocol on a Neoma MC-ICP-MS/MS, employing a ^{117}Sn–^{122}Sn double-spike and an ESI APEX Ω introduction system under dry plasma conditions, transmitted through the MS/MS system without additional mass-filtering or collision-cell processes. Furthermore, we propose an NaOH-based method to dissolve cassiterite, which is designed to provide a safe and efficient technique. We evaluate its performance alongside established digestion methods and external inter-laboratory comparisons.

2 Methods

2.1 Chemical reagents and labware

All chemical processing of samples was carried out in an ISO Class 5–6 cleanroom laboratory equipped with ISO Class 2–3 horizontal and vertical laminar flow exhaust workstations at Bayerisches Geoinstitut (BGI), University of Bayreuth. All sample and solution handling was conducted using pre-cleaned Savillex® Teflon perfluoroalkoxy (PFA) beakers, which were initially soaked in ~50% concentrated HNO_3 at 130 °C for 24 hours, followed by thorough rinsing and boiling in ultrapure Milli-Q water (resistivity: 18.2 MΩ cm^{-1}). NIST SRM 3161a (Lot# 140917; in 1% HF and 5% HNO_3) was used as the primary reference material for Sn isotope measurements, while an additional Sn ICP standard solution (Lot #9196150; in 20% HCl, Alfa Aesar) was employed as an in-house standard. The calibrated ^{117}Sn–^{122}Sn double spike used in this study was prepared at IPGP (Creech *et al.* 2017).[30] The cassiterite sample analyzed in this study originates from the Zinnwald deposit in Germany, one of the largest Li–Sn–W greisen systems in Europe. Mineralization is characterized by cassiterite occurring both within greisen bodies and together with wolframite in sub-horizontal quartz-rich veins.[58] The cassiterite grains are well euhedral, ranging from approximately 200 μm to 0.3 cm in size, allowing easy selection of pure cassiterite grains. The major element composition of cassiterite, determined by JEOL JXA-8200 EPMA at BGI, is listed in Table S1. Cassiterites commonly form clustered aggregates with quartz in quartz–cassiterite vein-type

mineralization. For the dissolution of cassiterite, sodium hydroxide powder (NaOH, ≥99%, Lot# 166233198; Carl Roth GmbH, Germany) was used. The solvent-impregnated resin TRU (TRU-B50-A, 100–150 μm, Eichrom, USA) was used for Sn purification. Geological reference materials BCR-2 (basalt, USGS, USA), BHVO-2 (basalt, USGS, USA), AGV-2 (andesite, USGS, USA), W-2 (diabase, USGS, USA), JA-2 (andesite, GSJ, Japan), and GSP-2 (granodiorite, USGS, USA) were used in this study for method development and calibration.

Procedural blanks were evaluated based on the measured Sn background in reagent solutions using ICP-MS. The Sn background measured in double-distilled 2% HNO_3 is ~10 ppt, comparable to the instrumental detection limit, and is reproducible across different batches of concentrated HNO_3 diluted to 2%. A slightly higher background (~15 ppt) is observed in 2% HCl, whereas high-purity HF contributes negligible Sn. Because the measured background is near the detection limit, acid-background values alone cannot be reliably scaled to estimate the total blank from the volumes of concentrated acids used during digestion. Nevertheless, given that typical samples contain Sn in the microgram range, the total blank contribution was calculated at max. 10 ng from the dissolution and chemistry procedure and kept <1% of the processed Sn to remain negligible for correction of measured isotopic compositions. Regarding the procedural blank associated with NaOH fusion, the NaOH reagent contains approximately 9 ng g^1 Sn. As ~1 g NaOH was used to dissolve ~100 mg cassiterite (corresponding to ~78 mg Sn), the NaOH-derived Sn contribution represents a negligeable fraction (<ppm) of the total Sn budget and cannot influence the isotopic results.

2.2 Sample digestion

Geological reference materials were digested in tightly capped Teflon beakers with a 3 : 1 mixture of concentrated HF and HNO_3 on a hotplate at 130 °C. ~1 μg of Sn from the samples (approximately 400 to 700 mg of rock powders) was digested to minimize the effects of contamination of Sn from the regents. The sample was mixed with the ^{117}Sn–^{122}Sn double spike solution before digestion, using an optimized spike-to-sample ratio of 40 : 60. During the 48-hour digestion, Sn released from the rock powders and equilibrated with the double spike. The solutions were then evaporated to dryness at 70 °C, redissolved and evaporated twice in concentrated HNO_3 and once in concentrated HCl, and finally re-dissolved in 2 mL of 0.5 M HCl in preparation for anion-exchange chromatography.

For cassiterite, an alkali fusion method was employed. Approximately 100 mg of finely ground cassiterite was thoroughly mixed with ten times its weight of NaOH and loaded into a MgO crucible (Fig. S1). The crucible was produced by machining a central cavity into a plate of commercial, dense MgO ceramics. This crucible was then inserted into a larger platinum crucible covered by a lid to contain volatile gases released during the reaction. The assembly was heated in a box furnace at 600 °C for 1–2 days (Fig. 1). The reaction process is represented in eqn (1):

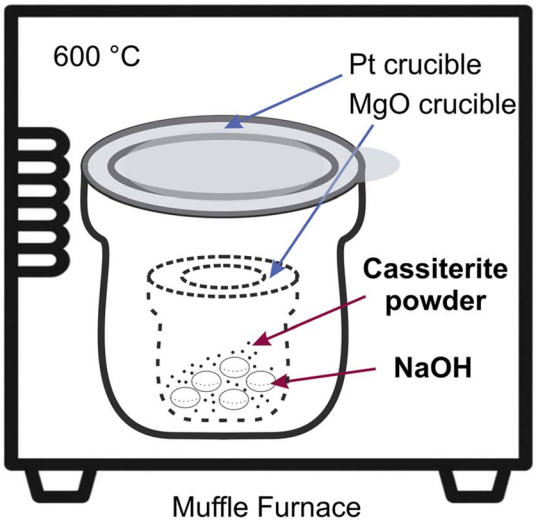

Fig. 1 Schematic illustration of cassiterite dissolution by alkaline fusion with NaOH. Fine-grained cassiterite powder mixed with NaOH was loaded into a MgO crucible, which was placed inside a Pt crucible covered with a Pt lid and heated at 600 °C in a muffle furnace for 3 days.

$$SnO_2(s) + 2\ NaOH(l) = Na_2SnO_3(s) + H_2O(g) \quad (1)$$

The resulting solid residues (Na_2SnO_3) were dissolved in three concentrated acids (HNO_3, HF, or HCl). The solutions were then diluted before determining Sn concentrations by ICP-MS. An aliquot corresponding to ~1 μg of Sn was mixed with the double spike, evaporated to dryness, and re-dissolved for isotope analysis, either directly or following column chemistry. Subsequently, all the prepared solutions were analyzed for Sn isotopes using a Neoma MC-ICP-MS/MS with or without Sn purification.

During the heating of the MgO crucible containing the NaOH and cassiterite, the surface of the surrounding Pt crucible and lid becomes etched by NaOH vapor. Most of this surface damage can be restored by subsequent heating of the empty Pt crucible in a furnace at 1000 °C. Alternatively, the outer Pt crucible could also be replaced by a commercial alumina crucible with an alumina lid, both to be disposed after each experiment. The possibility to dissolve cassiterite in molten NaOH is briefly mentioned – without any details – in some old textbooks of analytical chemistry.[59] Essential for the success of the method as described above is a very fine grain size (in the range of micrometers) of the cassiterite sample.

2.3 Chemical purification

The chemical separation of Sn in this study is based on established protocols employing 1.5 mL volume of Eichrom TRU resin contained in Biorad plastic columns.[29,30] Before sample loading, the resin was sequentially pre-cleaned with H_2O, 0.5 M HCl, and 2 × 0.5 M HNO_3, and then conditioned with 0.5 M HCl (see Table 1 for details). Following sample loading, matrix elements were eluted using 0.5 M and 0.25 M HCl, and Sn was subsequently recovered with 15 mL of 0.5 M HNO_3. The purified

Table 1 Chromatographic procedure for the separation of Sn using 1.5 mL Eichrom® TRU resin (100–150 μm)

Separation step	Reagent	Volume/mL
Cleaning	H_2O	5
	0.5 M HCl	5
	H_2O	5
	0.5 M HNO_3	5
	H_2O	5
	0.5 M HNO_3	5
	H_2O	5
Conditioning	0.5 M HCl	4
Loading	0.5 M HCl	2
Matrix elution	0.5 M HCl	4
	0.25 M HCl	7
Sn collection	0.5 M HNO_3	12

Sn fractions were then evaporated to dryness at 70 °C and redissolved in 1 mL of ~2% HNO_3 prior to isotopic analysis. Subsequently, an aliquot of 0.1 mL was taken and diluted tenfold to determine the intensity of ^{120}Sn. After matching the measured signal with that of the 50 ppb NIST SRM 3161a standard, the original solution was further diluted to achieve comparable signal intensity, ensuring that the intensity variation was kept within 15%.

2.4 Mass spectrometry

The Sn isotope measurements were performed on a Neoma™ MC-ICP-MS/MS (Thermo Fisher Scientific, Germany) setup at BGI. The instrumental operating conditions and measurement parameters are summarized in Table 2. The standard and sample solutions for isotope measurements were prepared with a concentration of 50 ng g^{-1} in 2% HNO_3 on the same day of the isotopic analysis. The sample was introduced into the ICP *via* an ESI APEX Omega desolvation nebulizer with a 100 μL min^{-1} PFA nebulizer, giving a sensitivity of ~24 V for ^{120}Sn. The measurements were conducted in low-resolution mode. Prior to analysis, instrumental tuning was performed to achieve maximum Sn sensitivity and a stable signal (0.1–0.2% RSD) for isotope ratio measurements. The torch position, nebulizer gas flow, and Ar make-up gas flow of the Apex Omega system were first iteratively adjusted to maximize signal intensity. Subsequently, the magnetic field and electric field, slits, and focus lenses (lenses 1–3) within the MS/MS system were optimized. The X-symmetry of focus lenses 1 and 3 was adjusted to obtain the highest sensitivity, while the Y-symmetry was tuned to improve signal stability. During the tuning process, the ^{122}Sn/^{118}Sn ratio was continuously monitored and adjusted to approach the theoretical value of 0.1913. In the final stage, minor adjustments of lens 2 base and the Y-symmetry of lens 3 were performed to ensure that the sensitivity decreased only slightly while maintaining an unchanged ^{122}Sn/^{118}Sn ratio. Each data acquisition sequence included 60 seconds of sample uptake followed by 40 cycles of 4 seconds signal integration on Faraday Cups. Procedural blanks were measured at the beginning of each analytical session and used to correct both the standards and the samples. To minimize memory effects and restore background levels, the sample introduction system was thoroughly rinsed between analyses using 2% HNO_3 from two separate tubes over a total duration of 10 minutes. Following this procedure, the background signal for Sn on the Neoma MC-ICP-MS/MS, evaluated at m/z 118, is <1 mV, more than three orders of magnitude lower than the typical sample signal and corresponding to a Sn background of <5 ppt in 2% HNO_3. Each sample measurement was bracketed by analyses of a spiked NIST SRM 3161a standard, with concentration matched to within 90–110% of those of the samples.

Table 2 Neoma MC-ICP-MS/MS settings for Sn isotope measurements

Parameter		Value
Apex Ω desolvating nebulizer system	N_2 flow	—
	Argon flow	1.8 to 2.2 L min^{-1}
	Spray chamber	140 °C
	Peltier cooling	3 °C
	Desolvator membrane	155 °C
	Nebulizer	MicroFlow PFA-100 μL min^{-1}
Measurement parameters	RF power	1200 W
	Plasma cooling gas flow rate	14 L min^{-1}
	Sampler cone	Ni jet type
	Skimmer cone	Ni X-type
	Detectors	Faraday cups
	Amplifiers	10^{11} Ω
	Instrument resolution	Low resolution
	Measurements	1 cycle × 40 repeats
	Integration time	4 s
	Solution concentration	50 ppb Sn
	Typical sensitivity	~1470 V ppm^{-1}
	Washout time	10 min

Cup configuration

L5	L4	L3	L2	L1	C	H1	H2	H3	H4	H5
^{111}Cd	^{115}Sn	^{116}Sn	^{117}Sn	^{118}Sn	^{119}Sn	^{120}Sn	^{121}Sb	^{122}Sn	^{123}Sb	^{124}Sn

Tin isotope ratios are reported in per mil (‰) notation relative to the NIST SRM 3161a Sn standard solution in this study:[60]

$$\delta^{122/118}Sn_{3161a} = [(^{122}Sn/^{118}Sn)_{sample}/(^{122}Sn/^{118}Sn)_{NIST\ 3161a} - 1] \times 1000$$

The effects of the NaOH-based digestion method of cassiterite on the measured Sn isotopic composition were evaluated against the KCN digestion method. Two samples of the same cassiterite were sent for isotopic analysis at the Curt-Engelhorn-Zentrum Archäometrie (CEZA) laboratory in Mannheim, Germany: one consisted of powdered cassiterite without any chemical pretreatment, which was digested using the KCN method at CEZA; the other was the product obtained from cassiterite treated by the NaOH-based digestion method at BGI. The KCN digestion and Sn isotope analytical procedures followed the technique described by Brügmann *et al.*[42] and Zhang *et al.*[61]

3 Results and discussion

3.1 Column chemistry

The Eichrom® TRU resin has been commonly employed as a highly efficient and reliable method for Sn purification from mineral and rock matrices,[23,29,30,42] even if several studies have introduced alternative two-step separation methods.[31,32,34,35,41] Previous studies have shown that Sn separation using TRU resin can achieve yields approaching ~100%,[23,29,42] and even when TRU is employed in combination with other resins in two-step ion-exchange procedures, recovery rates consistently exceed 80%.[34,35,41] However, the procedures used by Creech *et al.* (2017) (ref. 30) and Pathak and Mezger (2024) (ref. 31) resulted in substantial Sn loss, with recovery yields ranging from only 13–66% for TRU alone and 50–99% for cation exchange resin AG 50W-X8 in combination with TRU, respectively. She *et al.* (2023) suggested that a one-stage TRU column procedure is sufficient for processing geological samples,[29] which was also the reason we selected TRU resin for Sn purification. The use of a single-column procedure also reduces the likelihood of Sn loss and minimizes potential isotope fractionation during repeated evaporation steps. Elution profiles of matrix elements on TRU resin demonstrate that most matrix elements are effectively removed with 0.5 M HCl and 0.25 M HCl, while Sn is quantitatively recovered in the 0.5 M HNO_3 cut (Fig. 2). Only minor co-elution of Pt, Ag, and Zn was observed; however, their low abundance relative to Sn (Pt/Sn = 0.14, Ag/Sn = 0.28, and Zn/Sn = 0.26) indicates negligible effects on subsequent isotopic analysis. Previous experimental studies have further demonstrated that Ag and Zn do not introduce resolvable bias even at Ag/Sn or Zn/Sn ratios approaching unity.[29,30,34] In addition, Pt and Te are highly siderophile elements typically present at ultratrace abundances (ppb) in igneous samples, and are unlikely to contribute measurable matrix effects. Te, which could potentially cause isobaric interferences on Sn, is effectively separated during chromatography; the Te elution curve (Fig. 2) shows that ~99% of Te is removed during the HCl elution step prior to Sn collection. This observation is consistent with She *et al.*,[29] who demonstrated that a single-stage TRU column is sufficient for processing geological samples, in contrast to a two-stage protocol (TRU + AG1-X8). In our workflow, we capped the rock-powder load at less than 1 g per TRU column to limit matrix effects.

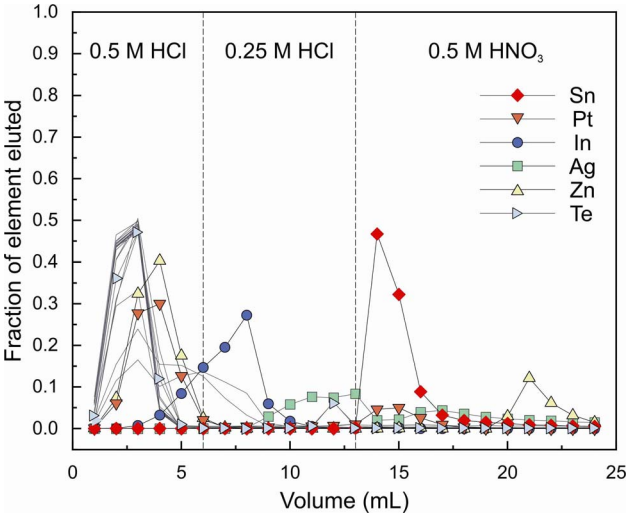

Fig. 2 Elution profiles of Sn and matrix elements during column chemistry chromatography using TRU resin. Matrix elements were sequentially eluted with 0.5 M HCl and 0.25 M HCl, while Sn was recovered in the 0.5 M HNO_3 fraction (~99%). The grey traces correspond to the unlabeled elements, including Mg, Al, Ca, V, Cr, Mn, Fe, Co, Ni, Cu, Ga, As, Rb, Sr, Ru, Pd, Cd, Sb, Ba, Hf, and Ir.

3.2 Double spike calibration and inversion

In this study, we employed the ^{117}Sn–^{122}Sn double spike composition established by Creech *et al.* (2017) through contour simulations, which identified an optimal configuration of 40% double spike in the spike–sample mixture with a balanced contribution of ^{117}Sn, yielding the lowest uncertainty in the natural fractionation factor α (Fig. S2). Using this double spike, we performed a four-isotope inversion with ^{117}Sn, ^{118}Sn, ^{122}Sn, and ^{124}Sn (^{118}Sn as the denominator), and simulations with the Double Spike Toolbox[62] confirmed that this configuration minimizes systematic error across a wide range of spike-to-total ratios, particularly between 0.2 and 0.75 (Fig. S3). The isotopic composition of the double spike was originally calibrated at IPGP and subsequently re-evaluated in our laboratory using the same Sb external normalization approach to correct for instrumental mass bias (Table S2). The calculated double spike isotope ratios, together with the corresponding ratios of NIST SRM 3161a, are listed in Table S2. To experimentally validate the calibration, we analyzed a series of mixtures between the double spike and the NIST SRM 3161a standard, with spike-to-sample ratios ranging from 40 : 60 to 60 : 40, which bracket the commonly adopted optimal mixing conditions. The corrected $\delta^{122/118}Sn$ values remained statistically indistinguishable from zero, falling within the typical external reproducibility and showing minimal internal errors with this range (Fig. 3 and

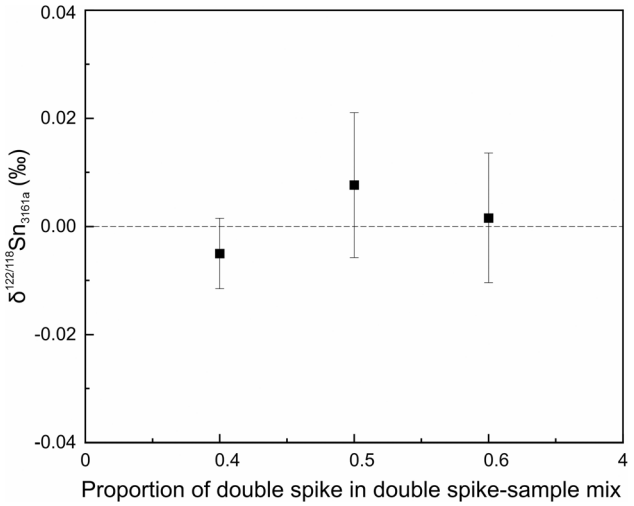

Fig. 3 $\delta^{122/118}Sn_{3161a}$ values of NIST 3161a after evaporation at different temperatures followed by re-dissolution. Each data point represents the average of three replicates (n = 3), with error bars showing 2SD.

Table S3). All double-spike calibrations were performed using a modified version of the DRS code from Creech *et al.*[63] implemented with the Isospike framework embedded in Iolite 4. The required input parameters include the three calibrated isotope ratios of the double spike ($^{117}Sn/^{118}Sn$, $^{122}Sn/^{118}Sn$, and $^{124}Sn/^{118}Sn$), as well as the corresponding three ratios for the NIST SRM 3161a standard solution. These parameters are used in the double spike inversion algorithm to correct for mass-dependent fractionation and accurately determine the true isotopic composition of the samples, using the exponential fractionation law.[62]

3.3 Evaporation effect (Sn loss)

Mass-dependent fractionation of Sn isotopes may occur during the sample preparation process, including both sample dissolution and chromatographic separation, as a result of volatile Sn loss. She *et al.* (2023) observed pronounced isotopic fractionation (~0.50‰ in $\delta^{124/116}Sn$) associated with around 90% Sn lost in HCl or HNO_3 solutions.[29] Previous studies have shown that the addition of an appreciable amount of HF (~100 μL) to evaporation solutions and the collected solution from column chemistry effectively suppresses Sn volatilization.[29,30,33] Qu *et al.*[35] evaluated the recovery efficiency of Sn in different acid combinations (concentrated HCl, concentrated HNO_3, 3 M HCl, 3 M HCl + 0.1 M HF, 2 M HNO_3, and 2 M HNO_3 + 0.1 M HF) for evaporation and re-dissolution tests. The results showed that Sn recoveries of 95–102% were achieved in 2 M HNO_3 + 0.1 M HF.[35] The strong electronegativity of F^- promotes the formation of stable $[SnF_6]^{2-}$, which exhibits high thermal stability (decomposing at ~705 °C) compared with the highly volatile $SnCl_4$ (114 °C).[35] In contrast, $Sn(NO_3)_4$ complexes are unstable and readily hydrolyze to insoluble SnO_2, thereby rendering HF an ideal additive. However, this design still presents a limitation: all tests were performed on pure Sn solutions without matrix components, preventing evaluation of matrix effects.

Understanding the mechanisms of Sn loss is crucial for reliable sample preparation and accurate Sn isotope measurements. Three ICP-MS calibration stock solutions were tested in this study: (1) a pure Sn solution (1 mL, 10 ppm), (2) a mixed solution containing 1 mL of 10 ppm Sn and 1 mL representative of a multi-element matrix solution (Ag, Al, As, Ba, Be, Bi, Ca, Cd, Co, Cr, Cs, Cu, Fe, Ga, In, K, Li, Mg, Mn, Na, Ni, Pb, Rb, Se, Sr, Tl, U, V, and Zn; each at 10 ppm), and (3) an ICP standard solution that inherently contained Sn (Au, Hf, Ir, Pd, Pt, Rh, Ru, Sb, Sn, and Te; 1 mL, 10 ppm). The initial solutions were stored in approximately 10% HCl. The recovery yields of Sn under different conditions are summarized in Fig. 4 and Table S4. For pure Sn solution, nearly complete recovery (~100%) was achieved after evaporation and re-dissolution at low temperatures (60 °C), whereas a marked decrease in yields was observed at 80 °C. In contrast, Sn solutions mixed with ICP matrix components exhibited somewhat improved recovery efficiency compared with pure Sn at the same temperature, although substantial losses of up to ~40% were observed at 120 °C. By

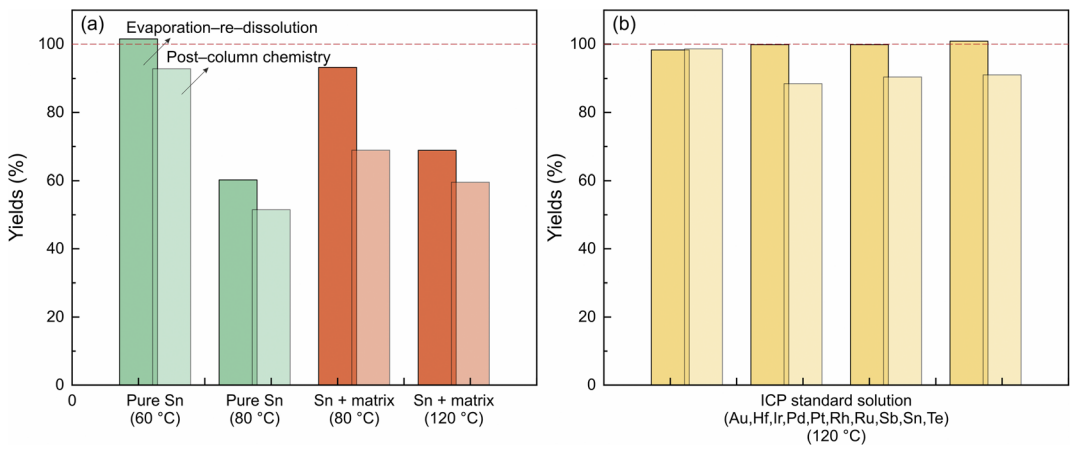

Fig. 4 Recovery yields of Sn after evaporation–re-dissolution and column chemistry. (a) Results for pure Sn solutions (60 °C and 80 °C) and Sn solutions with added matrix (80 °C and 120 °C). (b) Four replicate experiments using an ICP standard solution (containing Au, Hf, Ir, Pd, Pt, Rh, Ru, Sb, Sn, and Te) at 120 °C. The red dashed line denotes 100% recovery.

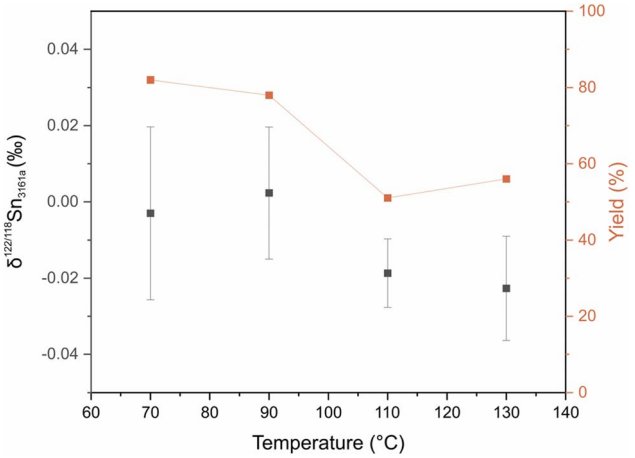

Fig. 5 $\delta^{122/118}Sn_{3161a}$ values and Sn recovery yields of NIST SRM 3161a after evaporation at different temperatures (70–130 °C). Error bars represent 2SD of replicate analyses ($n = 3$).

comparison, replicating tests using an ICP standard solution containing Sn (Au, Hf, Ir, Pd, Pt, Rh, Ru, Sb, Sn, and Te) consistently yielded high recoveries even at 120 °C (Fig. 4b). These results suggest that Sn loss is strongly dependent on the chemical environment during sample processing, with a homogeneous matrix-bearing solution providing more stable conditions, while the ion-exchange purification step remains the dominant source of Sn loss. This observation also accounts for the highly variable recoveries reported in previous studies.[23,29,30,42] It should be noted that the evaporation experiments were designed to evaluate Sn behavior under simplified and controlled chemical conditions relevant to analytical processing, rather than to reproduce the full compositional complexity of natural geological samples. The pronounced volatilization observed in single-element Sn solutions at elevated temperature (80–120 °C)[35] therefore represents an end-member scenario, highlighting the sensitivity of Sn to evaporation under unfavorable chemical conditions.

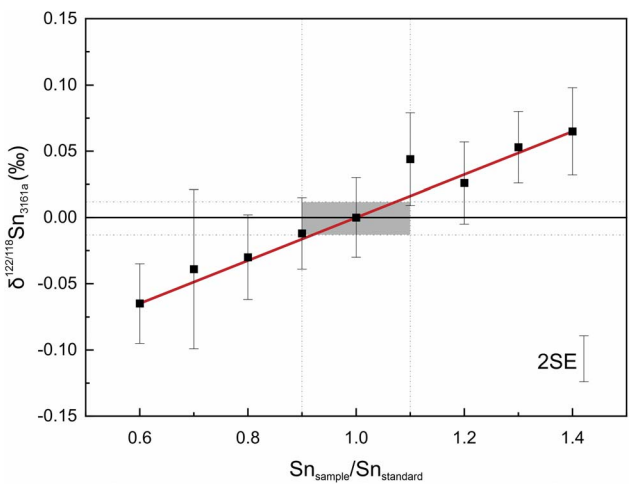

Fig. 6 Effect of concentration mismatch on $\delta^{122/118}Sn_{3161a}$. A positive linear relationship is observed, with δ offsets remaining within our long-term average standard deviation for isotopic measurements of ± 0.02‰ (grey band) when the concentration ratio lies between 0.90 and 1.10.

The NIST 3161a solutions were subjected to different tests, in which 1 μg of Sn was spiked with 0.667 μg of DS to achieve a 60 : 40 mass ratio (NIST 3161a: DS), thoroughly mixed, subsequently evaporated at different temperatures, and then re-dissolved. Because the sample and DS were heated together, this experiment simply examines the isotopic stability of the Sn–DS mixture during evaporation, as well as the corresponding Sn recovery. The $\delta^{122/118}Sn_{3161a}$ values remain stable below 90 °C, while slightly larger deviations appear at higher temperatures (Fig. 5 and Table S5), which correspond to decreasing Sn recovery yields. Although the DS-corrected results at 110–130 °C exhibit slight deviations, they fall well within the analytical uncertainty. The co-variation between yield and δ-values suggests that heating above ~100 °C may promote partial chemical transformation of dissolved Sn species, potentially leading to reduced solubility, although these effects remain minor within the investigated temperature range.

3.4 Effects of concentration mismatch

Isotopic deviations created by mismatches between the concentrations of the samples and of the bracketing standards have been reported for K, Fe, Ba, and Sn (ref. 29, 34 and 64–66). To assess potential effects of intensity mismatch, both bracketing standards (50 ng g^{-1}) and test solutions (30 to 70 ng g^{-1}) were prepared from a 1 μg g^{-1} NIST 3161a stock solution (Table S6). As shown in Fig. 6, the measured $\delta^{122/118}Sn_{3161a}$ values were plotted against the ratio of Sn concentration of the sample to that in the NIST 3161a standard, and the results reveal a clear positive linear relationship between sample Sn concentration and $\delta^{122/118}Sn_{3161a}$. Considering the overall trend, the relatively large deviation observed at $Sn_{sample}/Sn_{standard} = 1.1$ is most likely attributable to random analytical scatter rather than a systematic effect. An optimal concentration match within ± 0.10 between sample and standard solutions is required to constrain $\delta^{122/118}Sn_{3161a}$ offsets to less than 0.02‰, while Song *et al.*[34] demonstrated a broader applicable range of 0.5–1.5[34]. Nevertheless, as highlighted by She *et al.*,[29] the impact of concentration mismatch strongly depends on the instrumental configuration and double-spike settings, and may therefore differ across laboratories.

3.5 Measurement precision

Reproducibility tests for unprocessed Sn standard NIST 3161a (50 ng g^{-1}) analyzed using the double-spike technique demonstrate excellent intermediate precision over 8 months (Fig. 7a and Table S7). Over 8 months, the intermediate precision of $\delta^{122/118}Sn_{3161a}$ was ± 0.017‰ (2 SD, $n = 70$) (Fig. 7a), reflecting optimal instrumental performance. The intermediate precision (*i.e.*, reproducibility between different analytical sessions) was better than ± 0.02‰ for $\delta^{122/118}Sn_{3161a}$, which is comparable to previous studies: ± 0.05‰, Creech *et al.*;[30] ± 0.06‰, Wang *et al.*;[33] ± 0.04‰, She *et al.*;[29] ± 0.02‰, Pathak and Mezger;[31] ± 0.04‰, Song *et al.*[34] and 0.04–0.08‰, Qu *et al.*[35]

The Sn isotopic composition of another standard solution, Alfa ICP Sn standard, was also determined with the double

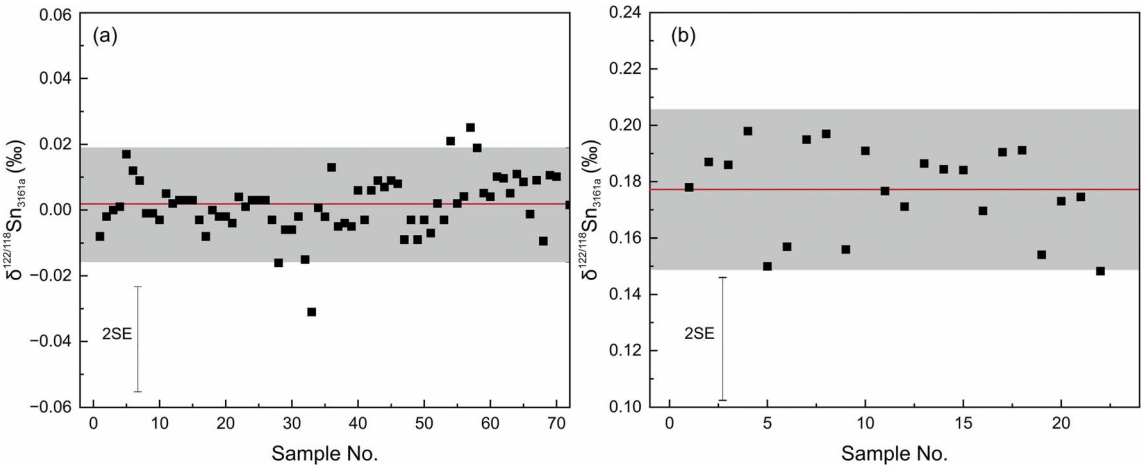

Fig. 7 Long-term reproducibility of Sn isotope analysis. (a) $\delta^{122/118}Sn_{3161a}$ values of the NIST 3161a standard monitored over 71 repeated measurements, yielding an average of 0.002 ± 0.017‰ (2SD). (b) $\delta^{122/118}Sn_{3161a}$ values of 22 repeated measurements of the ICP-MS Sn calibration solution, with a corresponding average of 0.177 ± 0.029‰ (2SD).

spike technique. The average $\delta^{122/118}Sn_{3161a}$ of Alfa Sn is 0.177 ± 0.029 (2SD, $n = 22$) (Fig. 7b), based on analyses performed over seven independent sessions, with two to four replicate measurements per session. Together, these results demonstrate that our double-spike method achieves high precision and reproducibility over both short- and long-term timescales, comparable to or better than previous studies, and is suitable for Sn isotope analysis of geological materials.

3.6 Tin isotopic compositions of geological reference materials

The Sn isotopic compositions (reported as $\delta^{122/118}Sn_{3161a}$) of a suite of widely used geological reference materials are shown in Fig. 8, with the corresponding data listed in Table 3. The results of this study are in good agreement with previously published data obtained on different MC-ICP-MS instruments (Neptune, Neptune Plus, Nu 1700 Sapphire, and Neoma). For basalt standards, BCR-2 and BHVO-2 yield $\delta^{122/118}Sn_{3161a}$ values

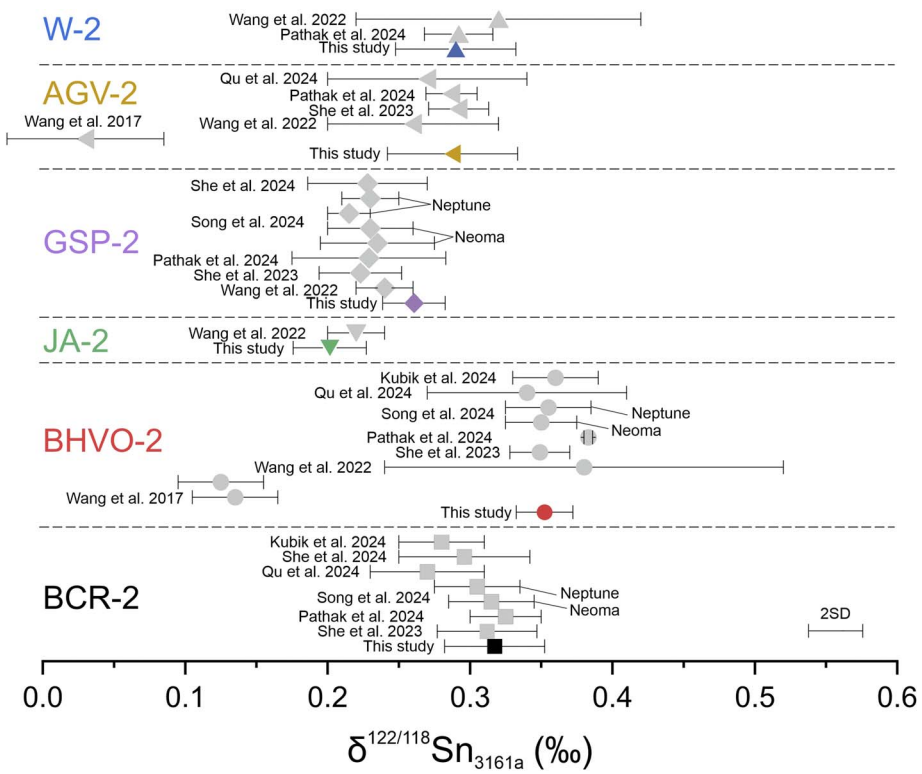

Fig. 8 Comparison of values for international geological reference materials (BCR-2, BHVO-2, JA-2, GSP-2, AGV-2, and W-2). Colored symbols represent results from this study, shown alongside previously published data in grey. Different reference materials are distinguished by different marker shapes. Errors in data reflect two standard deviations (2SD).

Table 3 $\delta^{122/118}Sn_{3161a}$ values of geological reference materials and standard solutions obtained in this study compared with previously published data

Sample	Lithology	Certified Sn concentration (μg g^{-1})	$\delta^{122/118}Sn_{3161a}$ (‰)	±	N[a]	Ref.
BCR-2 (USGS)	Basalt	2.28	0.317	0.035	13	This study
			0.312	0.035	9	She *et al.* (2023)
			0.325	0.025	4	Pathak and Mezger (2024)
			0.315	0.03	3	Neoma, Song *et al.* (2024)[b]
			0.305	0.03	6	Neptune, Song *et al.* (2024)[b]
			0.27	0.04	4	Qu *et al.* (2024)
			0.296	0.046	9	She *et al.* (2024)
			0.28	0.03	11	Kubik *et al.* (2024)
BHVO-2 (USGS)	Basalt	1.778	0.356	0.031	13	This study
			0.135	0.03	2	Wang *et al.* (2017)
			0.125	0.03	4	Wang *et al.* (2017)
			0.38	0.14	6	Wang *et al.* (2022)[c]
			0.349	0.021	8	She *et al.* (2023)
			0.383	0.003	5	Pathak and Mezger (2024)
			0.35	0.025	3	Neoma, Song *et al.* (2024)[b]
			0.355	0.03	3	Neptune, Song *et al.* (2024)[b]
			0.34	0.07	4	Qu *et al.* (2024)
			0.36	0.03	7	Kubik *et al.* (2024)
JA-2 (GSJ)	Andesite	1.68	0.202	0.026	8	This study
			0.22	0.02	6	Wang *et al.* (2022)[c]
GSP-2 (USGS)	Granodiorite	6.53	0.261	0.022	3	This study
			0.24	0.02	6	Wang *et al.* (2022)[c]
			0.223	0.029	12	She *et al.* (2023)
			0.229	0.054	6	Pathak and Mezger (2024)
			0.235	0.04	5	Neoma, Song *et al.* (2024) [c]
			0.23	0.03	4	Neoma, Song *et al.* (2024) [c]
			0.215	0.015	3	Neptune, Song *et al.* (2024) [c]
			0.23	0.02	3	Neptune, Song *et al.* (2024) [c]
			0.228	0.042	7	She *et al.* (2024)
AGV-2 (USGS)	Andesite	1.83	0.288	0.046	3	This study
			0.03	0.055	23	Wang *et al.* (2017)
			0.26	0.06	5	Wang *et al.* (2022)[c]
			0.292	0.021	5	She *et al.* (2023)
			0.287	0.018	6	Pathak and Mezger (2024)
			0.27	0.07	3	Qu *et al.* (2024)
W-2 (USGS)	Diabase	1.92	0.29	0.042	3	This study
			0.292	0.024	6	Pathak and Mezger (2024)
			0.32	0.1	5	Wang *et al.* (2022)[c]
NIST 3161a	Standard solution		0.002	0.017	70	This study
Alfa Sn	Standard solution		0.177	0.029	22	This study

[a] Repeatability for individual analyses is reported as 2SE, whereas for datasets with $n > 1$, the variability is expressed as 2SD. [b] Sn isotopic compositions given as $\delta^{124/116}Sn_{3161a}$ are reported as $\delta^{122/118}Sn_{3161a}$ by dividing the values by 2. [c] Sn isotopic compositions given as $\delta^{120/118}Sn_{3161a}$ are reported as $\delta^{122/118}Sn_{3161a}$ by multiplying by 2.

of 0.317 ± 0.035‰ and 0.352 ± 0.020‰ (2SD), respectively, consistent with earlier reports.[10,29,31,32,34,35] The $\delta^{122/118}Sn_{3161a}$ values of andesitic standards AGV-2 and JA-2 show slightly lower values of 0.287 ± 0.046‰ and 0.202 ± 0.026‰, respectively. GSP-2 and W-2 show comparable values within uncertainty. We do not include the Creech *et al.*[30] dataset in our interlaboratory comparison, as their measurements were reported against an earlier Sn_IPGP standard solution that is not directly comparable with the NIST SRM 3161a scale used here as no reliable conversion exists between the two bracketing solutions. Overall, our results confirm the accuracy and reproducibility of Sn isotope measurements of geological reference materials with those of other laboratories, showing no resolvable offset among datasets generated on different MC-ICP-MS platforms.

3.7 Dissolution efficiency of cassiterite by NaOH and implications for Sn isotope measurements

The recovery yields of the reaction products treated with different acids are summarized in Table 4. Comparable recovery

Table 4 Cassiterite dissolution yields obtained using different crucibles and post-treatment acids

Session	Sample no.	Crucible	Post-treatment acid	Yield (%)
# 1	1–1	MgO	HCl treated	69.58
	1–2	MgO	HNO_3 treated	<0.01
	1–3	MgO	HF treated	68.19
# 2	2–1	MgO	HCl treated	78.57
	2–2	Al oxide	HCl treated	89.39

Table 5 Sn isotopic compositions of cassiterite digestion using different methods (KCN- and NaOH-based) with/without Sn purification

Sample no.	Digestion method	Sn purification	$\delta^{122/118}Sn_{3161a}$ (‰)	2SD	δSn_{3161a} per amu (‰)	2SD	n	Lab
Cst-1	KCN-based	No	0.440[a]	0.008[b]	0.110	0.002	1	CEZA
Cst-2	NaOH-based	No	0.440[a]	0.004[b]	0.110	0.001	1	CEZA
Cst-3	NaOH-based	No	0.439	0.014[c]	0.110	0.003	4	BGI
Cst-4	NaOH-based	Yes	0.450	0.020[c]	0.112	0.005	8	BGI

[a] $\delta^{122/118}Sn_{3161a}$ were calculated from δSn_{3161a} per amu values using $\delta^{122/118}Sn_{3161a} = \delta Sn_{3161a}$ per amu × 4. [b] Internal analytical error of a single measurement (2SD) reported by CEZA Mannheim. [c] 2SD of replicate measurements obtained in this study (BGI).

yields of approximately 70% were obtained using HF and HCl. In contrast, re-dissolution in HNO_3 resulted in near-zero recovery, accompanied by the formation of visible black precipitates in the beaker. This is most plausibly attributed to the reaction of Na_2SnO_3 with HNO_3 and the subsequent reprecipitation of SnO_2, as shown in eqn (2):

$$Na_2SnO_3(s) + 2HNO_3(l) = SnO_2(s) + 2NaNO_3(l) + H_2O(l) \quad (2)$$

Additional experiments were carried out with different inner crucibles (MgO *vs.* Al oxide) to further evaluate the efficiency of our method to dissolve cassiterite without Sn loss. Additional details are provided in SI 1. The MgO crucible produced loose powdery residues, which could be recovered. The Al oxide crucible yielded products that adhered firmly to the bottom, complicating their extraction (Fig. S1). To address this, the entire Al oxide crucible was placed in a sealed 90 mL Teflon beaker with sufficient 6 M HCl and heated at 80 °C on a hot plate to leach Sn from the products. Although the experiments using an Al oxide crucible yielded a higher Sn recovery (89%) compared with the MgO crucible (79%) (Table 5), their use was discontinued due to operational complexity, the risk of contamination from HCl leaching, and frequent cracking during cooling. Consequently, MgO crucibles were employed in subsequent experiments.

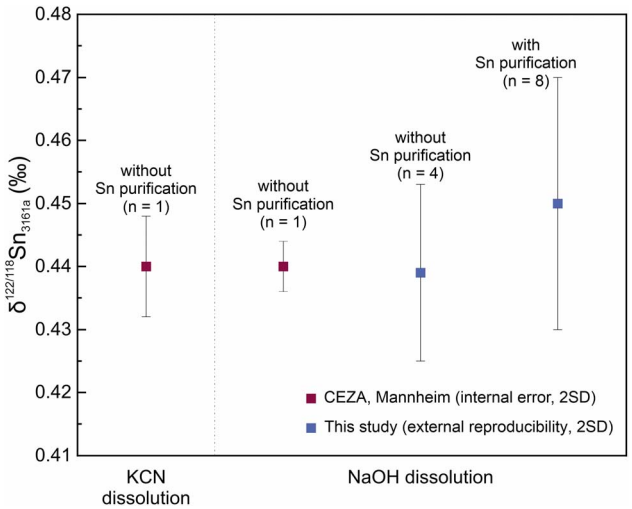

Fig. 9 $\delta^{122/118}Sn_{3161a}$ values of cassiterite dissolved using different methods (KCN *vs.* NaOH) with and without Sn purification. Red squares represent data from CEZA (Mannheim). Blue squares represent this study at BGI. Error bars for the CEZA Mannheim data represent the internal analytical errors of a single measurement (2SD), whereas those for this study represent the 2SD of replicate measurements of the cassiterite sample.

The Sn isotopic compositions of cassiterite samples obtained in this study are summarized in Table 5. Cassiterite samples dissolved using KCN and NaOH in the Mannheim laboratory yielded δSn_{3161a} values of 0.110 ± 0.002‰ and 0.110 ± 0.001‰ per amu (2SD) (Fig. 9), respectively, showing excellent consistency. Because the Mannheim data are reported as δSn_{3161a} per amu rather than in $\delta^{122/118}Sn_{3161a}$, they were converted to the $\delta^{122/118}Sn_{3161a}$ notation recommended by Meister *et al.*[60] by multiplying by the mass difference between ^{122}Sn and ^{118}Sn (*i.e.*, circa 4), ensuring consistent terminology throughout this study. The converted values are reported in Table 5. In our laboratory, $\delta^{122/118}Sn_{3161a}$ values of 0.439 ± 0.014‰ and 0.450 ± 0.020‰ were obtained for the same cassiterite sample (NaOH-treated) measured on a Neoma MC-ICP-MS/MS with and without Sn purification (Fig. 9), respectively, consistent with the results from the external laboratory. The agreement between purified and unpurified aliquots reflected the high purity of cassiterite (~99% SnO_2); after dissolution and dilution to 50 ppb, trace element concentrations were negligible and did not affect Sn isotope measurements. This consistency confirms the reliability of the NaOH dissolution method, the robustness of the purification protocol, and the analytical performance of the Neoma MC-ICP-MS/MS, thereby demonstrating the inter-laboratory comparability of Sn isotope measurements. Although *in situ* Sn isotope analysis is becoming increasingly common, providing high spatial resolution and micron-scale data with adequate precision,[42,46,51,53,54,61] suitable homogeneous and matrix-matched reference materials remain scarce. The NaOH-based cassiterite dissolution method and subsequent solution-based Sn isotope analysis developed in this study offer a faster, safer, and more accurate approach for cassiterite analysis and standard preparation.

4 Conclusions

An accurate and high-precision protocol for Sn analysis in geological materials was developed using the double spike technique and using a Neoma MC-ICP-MS/MS. Evaporation–re-dissolution tests demonstrate that matrix components play a key role in stabilizing Sn and minimizing losses, while single-stage TRU resin purification effectively removes matrix

elements with limited Sn loss (~10%) and without introducing measurable isotope fractionation. Concentration mismatch experiments reveal a clear dependence of $\delta^{122/118}Sn_{3161a}$ on the sample-to-standard concentration ratio, with $\delta^{122/118}Sn_{3161a}$ offsets constrained to < 0.02‰ when the ratio lies between 0.90 and 1.10. Long-term monitoring of NIST 3161a and an ICP Sn standard solution yielded external reproducibility values of 0.017‰ (2SD, $n = 70$) and 0.029‰ (2SD, $n = 22$), respectively. Analyses of geological reference materials further confirm that natural samples are consistent with previously published data. In addition, we demonstrate that cassiterite can be successfully decomposed by NaOH fusion, providing a safer and more practical alternative to conventional KCN digestion. This dissolution approach, combined with solution-based isotope analysis, thereby broadens the future application of Sn isotopes in ore deposit research, geochemistry, cosmochemistry, and archaeometallurgy.

Author contributions

Da-peng Zhu: data curation, formal analysis, visualization, writing – original draft; Edith Kubik: methodology, writing – review and editing; Hans Keppler: supervision, conceptualization, methodology; Audrey Bouvier: supervision, conceptualization, methodology, formal analysis, writing – review and editing, validation, funding.

Conflicts of interest

There are no conflicts of interest to declare.

Data availability

The data that support the findings of this study are available in the supplementary information (SI) of this article. Supplementary information is available. See DOI: https://doi.org/10.1039/d5ja00507h.

Acknowledgements

This work was financially supported by the Deutsche Forschungsgemeinschaft (DFG, Grants INST 91/455-1 for LA-MC-ICPMS/MS instrumentation to AB), the University of Bayreuth, and the Bayerisches Geoinstitut for instrumentation and analyses. Dapeng Zhu thanks the China Scholarship Council (No. 202206370044) for financial support. We thank Jiaxin She, John Creech, Remco Hin, and Bence Paul for discussion about the double spike methodology. We deeply thank Frédéric Moynier and Klaus Mezger for providing the double spike, NIST solutions, and geological reference standard materials to enable the development of this study at BGI. We also thank Charlie Palmer (Publishing Editor) and two anonymous reviewers for their constructive comments, which have helped improve the manuscript.

References

1 C. A. Heinrich, *Econ. Geol.*, 1990, **85**, 457–481.
2 G. Witt-Eickschen, H. Palme, H. St. C. O'Neill and C. M. Allen, *Geochim. Cosmochim. Acta*, 2009, **73**, 1755–1778.
3 E. Kubik, J. Siebert, B. Mahan, J. Creech, I. Blanchard, A. Agranier, S. Shcheka and F. Moynier, *J. Geophys. Res.:Solid Earth*, 2021, **126**, e2021JB022026.
4 X. Wang, C. Fitoussi, B. Bourdon, B. Fegley and S. Charnoz, *Nat. Geosci.*, 2019, **12**, 707–711.
5 X. Wang, O. Nebel, A. Churchus and P. A. Cawood, *Geochim. Cosmochim. Acta*, 2025, **399**, 18–34.
6 X. Wang, C. Fitoussi, B. Bourdon, K. Righter and Q. Amet, *Geochim. Cosmochim. Acta*, 2021, **312**, 139–157.
7 J.-X. She, W. Li, S. Zhang, C. Gu, X. Chen, H. Zheng, C. Xu and W. Liu, *Proc. Natl. Acad. Sci. U. S. A*, 2025, **122**, e2504065122.
8 J.-X. She, W. Li, E. Kubik, F. Moynier, X.-L. Luo, J. Mu, S. An, C.-Z. Wu, Z. Hu and J. Ji, *Geochim. Cosmochim. Acta*, 2024, **381**, 43–59.
9 Y. Fukami, R. Ariizumi, Y. Ijichi, T. Ohno, T. Kashiwabara, T. Shibuya, K. Suzuki and T. Hirata, *Proc. Natl. Acad. Sci. U. S. A*, 2024, **121**, e2321616121.
10 E. Kubik, F. Moynier, J.-X. She and R. L. Rudnick, *Geochem. Perspect. Lett.*, 2024, **30**, 51–56.
11 W. Powell, M. Frachetti, C. Pulak, H. A. Bankoff, G. Barjamovic, M. Johnson, R. Mathur, V. C. Pigott, M. Price and K. A. Yener, *Sci. Adv.*, 2022, **8**, eabq3766.
12 W. Powell, K. A. Yener, G. Barjamovic, F. Kulakoğlu, E. Yazgan and R. Mathur, *J. Archaeol. Sci.*, 2024, **162**, 105917.
13 P. Carr, M. D. Norman, V. C. Bennett and P. L. Blevin, *Econ. Geol.*, 2021, **116**, 147–167.
14 K.-K. Sun, J.-X. She, D.-H. Du, W. Li and J. Deng, *Chem. Geol.*, 2023, 121843.
15 J. G. Wiederhold, *Environ. Sci. Technol.*, 2015, **49**, 2606–2624.
16 V. N. Epov, D. Malinovskiy, F. Vanhaecke, D. Bégué and O. F. X. Donard, *J. Anal. At. Spectrom.*, 2011, **26**, 1142.
17 A. Bragagni, F. Wombacher, M. Kirchenbaur, N. Braukmüller and C. Münker, *Geochim. Cosmochim. Acta*, 2023, **344**, 40–58.
18 F. Moynier, T. Fujii and P. Telouk, *Anal. Chim. Acta*, 2009, **632**, 234–239.
19 A. Audétat, *Econ. Geol.*, 2019, **114**, 1033–1056.
20 H. Keppler and A. Audétat, *Geochim. Cosmochim. Acta*, 2025, **394**, 182–193.
21 Q. Duc-Tin, A. Audétat and H. Keppler, *Geochim. Cosmochim. Acta*, 2007, **71**, 3323–3335.
22 Z.-H. Zhou, J.-W. Mao, J.-Q. Zhao, X. Gao, S. Weyer, I. Horn, F. Holtz, P. A. Sossi and D.-C. Wang, *Am. Mineral.*, 2022, **107**, 2111–2127.
23 E. Yamazaki, S. Nakai, T. Yokoyama, S. Ishihara and H. Tang, *Geochem. J.*, 2013, **47**, 21–35.
24 N. H. Gale, *Archaeometry*, 1997, **39**, 71–82.
25 N. J. McNaughton and K. J. R. Rosman, *Geochim. Cosmochim. Acta*, 1991, **55**, 499–504.

26 K. J. R. Rosman and N. J. McNaughton, *Int. J. Mass Spectrom. Ion Processes*, 1987, **75**, 91–98.
27 C. Devillers, T. Lecomte and R. Hagemann, *Int. J. Mass Spectrom. Ion Phys.*, 1983, **50**, 205–217.
28 W. Yi, A. N. Halliday, D.-C. Lee and J. N. Christensen, *Geochim. Cosmochim. Acta*, 1995, **59**, 5081–5090.
29 J.-X. She, W. Li, S. An and Y. Cai, *J. Anal. At. Spectrom.*, 2023, **38**, 142–155.
30 J. B. Creech, F. Moynier and N. Badullovich, *Chem. Geol.*, 2017, **457**, 61–67.
31 D. Pathak and K. Mezger, *Geostand. Geoanal. Res.*, 2024, 12575.
32 Z.-Y. Wang, Z.-Y. Luo, L. Zhang, J.-J. Liu and J. Li, *Geostand. Geoanal. Res.*, 2022, **46**, 547–561.
33 X. Wang, C. Fitoussi, B. Bourdon and Q. Amet, *J. Anal. At. Spectrom.*, 2017, **32**, 1009–1019.
34 W. Song, C. Zhu, H. Wen, Y. Zhang, Z. Liu and M. Zhou, *Geostand. Geoanal. Res.*, 2024, 12590.
35 Q. Qu, W. Liu, W. Zheng, B. Chetelat, Q. Liu and J. Chen, *J. Anal. At. Spectrom.*, 2024, **39**, 2258–2269.
36 X. Li, Y. He, S. Ke, A.-Y. Sun, Y.-C. Zhang, Y. Wang, R.-Y. Yang and P.-J. Wang, *At. Spectrosc.*, 2022, **43**, 164–173.
37 G. Wu, J.-M. Zhu, X. Wang, G. Han, D. Tan and S.-J. Wang, *J. Anal. At. Spectrom.*, 2019, **34**, 1639–1651.
38 Q. Amet and C. Fitoussi, *Int. J. Mass Spectrom.*, 2020, **457**, 116413.
39 E. Wölfer, C. Burkhardt and T. Kleine, *J. Anal. At. Spectrom.*, 2025, **40**, 1023–1036.
40 B. Andris and J. Beňa, *J. Radioanal. Nucl. Chem.*, 2016, **308**, 781–788.
41 M. Friebel, E. R. Toth, M. A. Fehr and M. Schönbächler, *J. Anal. At. Spectrom.*, 2020, **35**, 273–292.
42 G. Brügmann, D. Berger and E. Pernicka, *Geostand. Geoanal. Res.*, 2017, **41**, 437–448.
43 J. M. Bennett, A. I. S. Kemp and M. P. Roberts, *Am. Mineral.*, 2020, **105**, 58–76.
44 J. M. Bennett, A. I. S. Kemp, S. G. Hagemann, M. L. Fiorentini and M. P. Roberts, *Aust. J. Earth Sci.*, 2024, **71**, 1098–1124.
45 P. Bhalla, F. Holtz, R. L. Linnen and H. Behrens, *Lithos*, 2005, **80**, 387–400.
46 J.-X. She, W. Li, S. An, T. Yang and R. Zhang, *J. Anal. At. Spectrom.*, 2023, **38**, 1043–1056.
47 Y. Cheng, C. Spandler, A. Kemp, J. Mao, B. Rusk, Y. Hu and K. Blake, *Am. Mineral.*, 2019, **104**, 118–129.
48 L. Han, J.-Y. Pan, P. Ni and H. Chen, *Geochim. Cosmochim. Acta*, 2023, **342**, 108–127.
49 X. Liu, P. Yu and C. Xiao, *Geosci. Front.*, 2023, **14**, 101624.
50 Z. Luo, H. Li, M. Ghaderi, D. Zhu, W. Jiang and J. Wu, *Int. Geol. Rev.*, 2024, 1–24.
51 D.-Y. Xiong, X.-L. Wang, A. Hofmann, W. Li, R.-Q. Zhang, T. Nazari-Dehkordi, Y. Guan and S.-C. An, *Commun. Earth Environ.*, 2024, **5**, 785.
52 R. Mathur, W. Powell, J. Yao, F. Guimaraes, Y. Cheng, L. Godfrey, F. Tornos, D. Killick, J. Stephens, J. Mao, M. Sun and B. Lehmann, *Geosciences*, 2025, **15**, 28.
53 J. Yao, R. Mathur, W. Powell, B. Lehmann, F. Tornos, M. Wilson and J. Ruiz, *Am. Mineral.*, 2018, **103**, 1591–1598.
54 P. Liu, J. Mao, B. Lehmann, S. Weyer, I. Horn, R. Mathur, F. Wang and Z. Zhou, *Am. Mineral.*, 2021, **106**, 1980–1986.
55 R. Clayton, P. Andersson, N. H. Gale, C. Gillis and M. J. Whitehouse, *J. Anal. At. Spectrom.*, 2002, **17**, 1248–1256.
56 D. Berger, G. Brügmann and E. Pernicka, *Archaeol. Anthropol. Sci.*, 2019, **11**, 293–319.
57 R. Mathur, W. Powell, A. Mason, L. Godfrey, J. Yao and M. E. Baker, *Geostand. Geoanal. Res.*, 2017, **41**, 701–707.
58 M. Korges, P. Weis, V. Lüders and O. Laurent, *Geology*, 2018, **46**, 75–78.
59 G. Jander and E. Blasius, *Lehrbuch der analytischen und präparativen anorganischen Chemie*, Hirzel, 4. neubearb, Aufl, 1979, 529–538.
60 A. C. E. Meister, M. A. Fehr, Q. Amet, G. Brügmann, C. Fitoussi, M. Friebel, W. Li, F. Moynier, J.-X. She, X. Wang and M. Schönbächler, *Geostand. Geoanal. Res.*, 2026, DOI: 10.1111/ggr.70035.
61 D. Zhang, Z. Bao, P. Liu, G. Brügmann, W. Yang, K. Chen, P. Liang and H. Yuan, *J. Anal. At. Spectrom.*, 2023, **38**, 204–211.
62 J. F. Rudge, B. C. Reynolds and B. Bourdon, *Chem. Geol.*, 2009, **265**, 420–431.
63 J. B. Creech and B. Paul, *Geostand. Geoanal. Res.*, 2015, **39**, 7–15.
64 K. Chen, Z. Bao, H. Yuan and N. Lv, *J. Anal. At. Spectrom.*, 2022, **37**, 249–263.
65 P. Télouk, E. Albalat, T. Tacail, F. Arnaud-Godet and V. Balter, *J. Anal. At. Spectrom.*, 2022, **37**, 1259–1264.
66 X. Nan, F. Wu, Z. Zhang, Z. Hou, F. Huang and H. Yu, *J. Anal. At. Spectrom.*, 2015, **30**, 2307–2315.

